JOURNAL OF PHYSICAL ORGANIC CHEMISTRY
J. Phys. Org. Chem. 2004; **17:** 199–206
Published online in Wiley InterScience (www.interscience.wiley.com). DOI: 10.1002/poc.714

Photophysics of Poly{2,2′-bipyridine-5,5′-diylethynylene [2,5-di(2-ethylhexyl)oxy-1,4-phenylene]ethynylene}: a comparison with monomer and dimer model compounds

U.-W. Grummt,[1]* Th. Pautzsch,[2] E. Birckner,[1] H. Sauerbrey,[1] A. Utterodt,[1] U. Neugebauer[1] and E. Klemm[2]

[1]Institut für Physikalische Chemie, Friedrich-Schiller-Universität Jena, Lessingstrasse 10, D-07743 Jena, Germany
[2]Institut für Organische und Makromolekulare Chemie, Friedrich-Schiller-Universität Jena, Humboldtstrasse 10, D-07743 Jena, Germany

Received 12 May 2003; revised 11 July 2003; accepted 8 August 2003

epoc ABSTRACT: The title compound (**P**) was synthesized via Pd- and Cu-catalyzed coupling reactions (Sonogashira reaction). Two model compounds prepared by similar synthetic routes, 1,4-bis(2,2′-bipyridin-5′-ylethynyl)-2,5-di(2-ethylhexyl)oxybenzene (**M**), and 5,5′-[1-ethynyl-4-(2,2′-bipyridin-5′-ylethynyl)-2,5-di(2-ethylhexyl)oxybenzene]-2,2′-bipyridine (**D**), were included in the spectroscopic investigations for comparison. As a result of steady-state and time-resolved absorption and fluorescence investigations in solution and in solid films, we conclude that the π-conjugation is restricted by torsional motions of the aromatic chain segments at ordinary temperature. It comprises about 2–3 repetition units in the S_1 state as concluded from a comparison of the experimental radiative rate constant with that calculated from the Strickler–Berg relation. It is even less in the ground state. The theoretical limit obtained from DFT calculations is about twice as large for the ideal coplanar conformation. Whereas the π–π stacking interaction in pure polymer films is very weak in the ground state, it is significantly stronger in the S_1 state, giving rise to excimer fluorescence. Energy migration along the polymer backbone is inefficient. Intermolecular energy migration and transfer to embedded acceptors becomes efficient in solid films. Copyright © 2004 John Wiley & Sons, Ltd.
Additional material for this paper is available in Wiley Interscience.

KEYWORDS: 2,2′-bipyridine, conjugated polymers; energy migration; fluorescence; photophysics

INTRODUCTION

Conjugated polymers have recently been the focus of considerable interest owing to their potential applications as electroluminescent materials,[1] as photoactive materials for the construction of a second generation of solar cells[2] and as molecular wires[3] and also because of their large optical non-linearities.[4–6] Polymers with *N*-heterocycles in the backbone exhibit a higher oxidation potential, which makes them more stable against oxidation, an advantage in application as electroluminescent materials. Among these *N*-heterocycles, 2,2-bipyridine and 1,10-phenanthroline are particularly important owing to their metal chelating properties.[7] Ley and co-workers reported the first synthesis of and photophysical data for a polymer containing 2,2′-bipyridylethynylene in the backbone.[8] In preceding papers,[9–11] we reported the absorption and emission spectra of new linear and angular conjugated polymers, oligomers and their model compounds, all of which contain 2,2′-bipyridine and diethynylenebenzene units in their backbone. From the viewpoint of basic rather than applied research, segmented conjugated polyarenes are useful objects for investigating energy migration along the polymer chain.[12,13] For instance, the antenna effect could be exploited in order to enhance significantly the sensitivity of a fluorescent chemosensor.[14] In particular, fluorescent rigid rod oligomers and their model compounds are excellent probes for studying molecular motions in viscous media via static and kinetic monitoring of the fluorescence anisotropy.

Understanding the photophysics as a function of the chemical structure is one prerequisite for the chemical design of optimized luminescent polymers for practical application. Low molecular weight model compounds and monodisperse oligomers are indispensible for that purpose.[15]

In this paper, we report the synthesis of and photophysical data for a polymer and of two low molecular weight model compounds. The model compounds consist of one or two repetition units and are end-capped by 2,2′-bipyridin-5-yl units. For convenience we shall call them ‘monomer’ and ‘dimer’, respectively. The structures of the compounds are shown in Scheme 1.

**Correspondence to:* U.-W. Grummt, Institut für Physikalische Chemie, Friedrich-Schiller-Universität Jena, Lessingstrasse 10, D-07743 Jena, Germany.
E-mail: cug@uni-jena.de

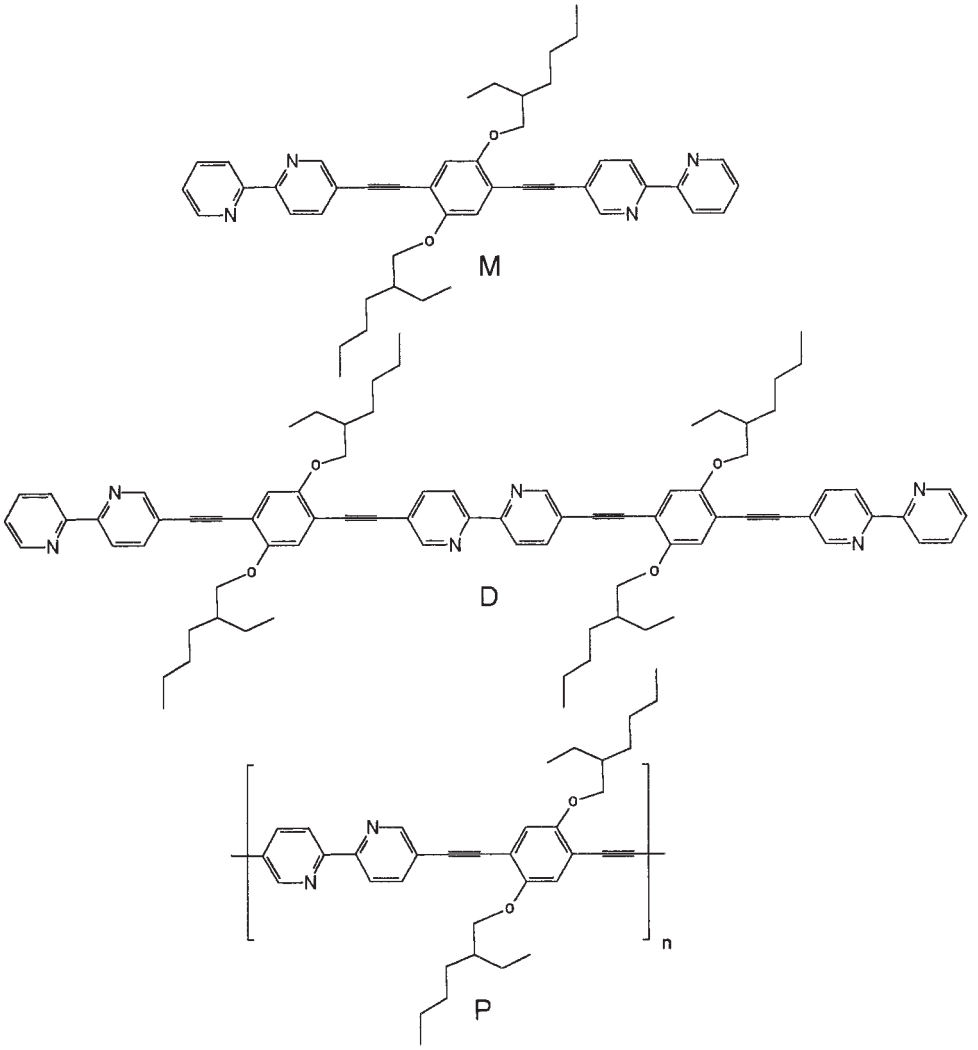

Scheme 1

EXPERIMENTAL

Synthesis

The syntheses of the 'monomer' and 'dimer' model compounds, 1,4-bis(2,2′-bipyridin-5′-ylethynyl)-2,5-di(2-ethylhexyl)oxybenzene (**M**) and 5,5′-[1-ethynyl-4-(2,2′-bipyridin-5′-ylethynyl)-2,5-di(2-ethylhexyl)oxybenzene]-2,2′-bipyridine (**D**), have been described elsewhere.[16] Poly{2,2′-bipyridine-5,5′-diylethynylene[2,5-di(2-ethylhexyl)oxy-1,4-phenylene]ethynylene} (**P**) was synthesized via Pd- and Cu-catalyzed Sonogashira coupling reactions. The detailed procedure and analytical data are given in the supplementary material, available at the epoc website at http://www.wiley.com/epoc.

Instrumentation

Molar absorptivities were determined in $CHCl_3$ and/or 1,4-dioxane (HPLC quality; Baker) on a Perkin-Elmer Lambda 19 UV/VIS-NIR spectrometer. Spectroscopic-grade solvents (Uvasol; Merck) were used for all other spectroscopic investigations. Absorption spectra were recorded on a Lambda 16 spectrophotometer (Perkin-Elmer). Corrected fluorescence emission and excitation spectra were measured using an LS50B luminescence spectrometer (Perkin-Elmer). The emission spectra presented were recorded with excitation at the longest wavelength absorption maximum. Fluorescence excitation spectra were measured at various emission wavelengths in order to prove the purity of the compounds. The spectral slit widths of both the emission and excitation monochromators were set to 4 nm for all measurements. Low-temperature experiments recorded at 77 K used the low-temperature accessory of the LS50B spectrometer and were performed with samples that had been placed in fused synthetic silica tubes of 2 mm inner diameter. Fluorescence quantum yields (error $<\pm 10\%$) were calculated relative to quinine sulfate (purum; Fluka) in 0.1 N H_2SO_4 (pro analysi; Laborchemie Apolda) used as a standard ($\Phi_f = 0.55$).[17] The absorbance at the excitation

wavelength was kept below 0.05 for the samples and the reference. The fluorescence kinetics with sub-nanosecond time resolution was investigated with a CD900 time-correlating single photon counting spectrometer (Edinburgh Instruments). The excitation source was a hydrogen-filled nanosecond flashlamp which allowed the variation of the excitation wavelength. The instrument response pulse had an FWHM of 1.3 ns. Polarizers with a vertical orientation on the excitation side and a 55° (magic angle) orientation on the emission side were used to avoid polarization effects. The kinetics of fluorescence were recorded at the emission maxima under excitation at the longest wavelength absorption maxima. Decay curves were accumulated until 10^4 counts at the maximum with at least 10^3 occupied channels. The channel width corresponded to 13 ps.

Picosecond time-resolved fluorescence polarization measurements were performed with an apparatus consisting of a frequency-doubled mode-locked titanium–sapphire laser (100 fs, 104 MHz, 400 nm) as the excitation source and a Hamamatsu microchannel plate photomultiplier (MCP-PMT R3809U-50) and an SPC-430 single photon counting board (Becker and Hickl, Berlin, Germany) as the detecting unit. The synchronization signal for the SPC circuit was generated by a fast photodiode (PHD-400) exposed to a small fraction of the excitation pulses. A 90° excitation/emission geometry was applied. Identical monochromators (Sciencetech 9030) used for excitation and emission are part of the optical equipment. A Glan–Tompson prism can optionally be inserted between the monochromators and the sample compartment. The width (FWHM) of the instrument pulse is 35 ps due to the rise time of the photomultiplier. Polarized fluorescence decay curves were accumulated until 64000 counts at the maximum with at least 3000 occupied channels (channel width 2.44 ps). 4-Dimethylamino-4′-cyanostilbene (DCS) in cyclohexane at 25 °C was used as a reference substance for testing the performance. We found a lifetime of 66.4 ps, which is in excellent agreement with the literature.[18] Emission anisotropy measurements were performed in the usual manner as described by Lakowicz.[19] The correct alignment of the polarizers was tested with the help of a Ludox suspension (Grace Davison, Columbia, USA) at the excitation wavelength of 400 nm. We found an emission anisotropy of $r = 0.98 \pm 0.02$ for the scattered light.

In order to calculate the fluorescence lifetime, the LEVEL 1 (up to four exponentials) and LEVEL 2 (Distribution Analysis, Spherical Rotor) packages implemented in the Edinburgh Instruments software were used. (The analysis makes use of the iterative reconvolution technique and the Marquardt fitting algorithm.) Plots of weighted residuals and of the autocorrelation function and values of reduced residuals χ^2 were used to judge the quality of the fit, χ^2 values larger than 1.4 were not accepted. The error of the lifetimes (single exponential) was <50 ps and <5 ps for the CD900 and the SPC430 data, respectively. The Edinburgh Instruments software was used to calculate the fundamental anisotropies from the experimental time-resolved anisotropy curves.

Films were prepared by spin coating (P6204, Speciality Coating Systems, Indianapolis, IN, USA) from chloroform solutions (1–3 mg ml^{-1}) at 2000 rpm, producing layers of about 10 nm thickness for the pure films as estimated from their absorption.

Computations

The Gaussian 98 package[20] was used for geometry optimizations and TDDFT (time-dependent density functional theory) calculations. The hybrid b3lyp/6–31+g(d) basis set was applied. Frequency calculations confirmed that true minima were found if not stated otherwise.

RESULTS AND DISCUSSION

Absorption and fluorescence in fluid solution

Absorption spectra. Figure 1 shows the normalized absorption and fluorescence spectra of **M**, **D** and **P** in dioxane as solvent at room temperature. Photophysical data for **M**, **D** and **P** are given in Table 1 for the solvents dioxane and chloroform.

The molar absorptivities of the longest wavelength transition increase linearly with the number of repetition units. The molar absorptivity of **P** normalized to one repetition unit is well reproduced with the model compounds **M** and **D**. These findings underline that the repetition unit as depicted in Scheme 1 is indeed the essential chromophore unit for the absorption at least for solutions at room temperature. As is obvious from Fig. 1, the wavelength of the absorption and fluorescence maxima of the 'dimer' has almost converged to the values for the polymer. Therefore, additional synthetic effort to prepare larger oligomers may not be justified. Instead, we calculated transition data for a slightly larger series of model compounds **1**–**4** where the index n in the formula (Fig. 2) serves as the substance code. The TDDFT results for the $S_1 \leftarrow S_0$ transitions are shown in Fig. 2. Exponential fits of the theoretical absorption wavelengths extrapolate to 522 nm for infinite chain length.

Because of low torsional barriers for motions around the ethynylene linkage,[21] the effect of non-coplanarity was also theoretically investigated. Figure 3 shows the torsional energy profile for **2** around the central ethynylene linkage. The two parts of the molecule were kept coplanar. Also included is the position of the absorption maximum. The oscillator strength parallels qualitatively the curve of λ_{max} with $f = 3.1$ and 1.5 for 0 and 90°, respectively.

The barrier amounts to 5.8 kJ mol^{-1}, which is significantly larger than that obtained for tolane calculated earlier as 3.4 kJ mol^{-1} [B3LYP/6–31+G(d)].[21] This

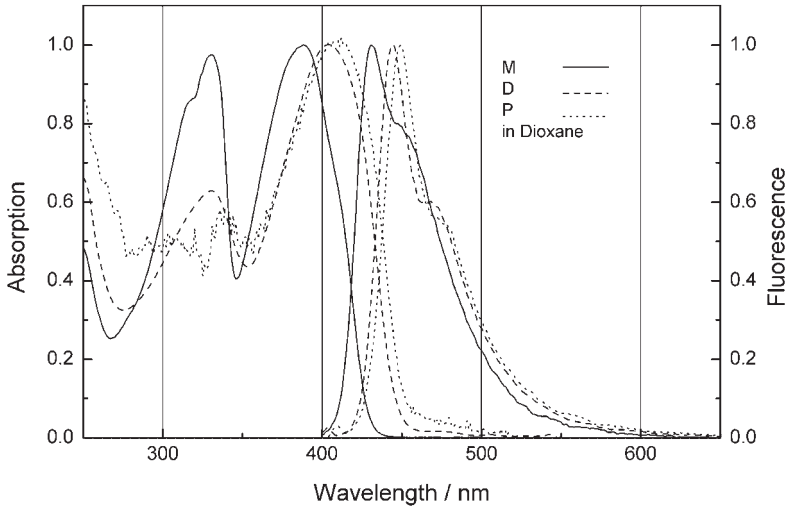

Figure 1. Normalized absorption and emission spectra of **M**, **D** and **P** in dioxane solution at room temperature

Table 1. Photophysical data in dioxane and chloroform at room temperature

Parameter[a]	Solvent	**M**	**D**	**P**
λ_a(nm)	Dioxane	389	404	412
	$CHCl_3$	390	407	420
$\varepsilon(M^{-1}\,cm^{-1})$	$CHCl_3$	52100	110000	40900[b]
λ_f(nm)	Dioxane	431	445	450
	$CHCl_3$	437	452	457
$\Delta\nu$ (cm^{-1})	Dioxane	2500	2280	2050
	$CHCl_3$	2760	2450	1930
ϕ_f	Dioxane	0.90	0.93	0.77
	$CHCl_3$	0.92	0.91	0.64
τ (ns)	Dioxane	1.35	0.90	0.76
	$CHCl_3$	1.25	0.98	0.74
ϕ_f/τ (ns^{-1})	Dioxane	0.67	1.1	1
	$CHCl_3$	0.74	0.93	0.86
k_f (SB)/(ns^{-1})	$CHCl_3$	0.47	1.23	0.39
$k_{nr} = (1-\phi_f)/\tau$ (ns^{-1})	Dioxane	0.074	0.078	0.30
	$CHCl_3$	0.064	0.092	0.48

[a] λ_a, λ_f Wavelengths of the absorption and fluorescence maxima, respectively ϵ, molar absorptivity; $\Delta\nu$, Stokes shift; ϕ_f, τ, fluorescence quantum yield and lifetime, respectively; k_f (SB), radiative rate determined after Strickler and Berg; k_{nr}, non-radiative decay rate.
[b] Calculated for one repetition unit.

clearly demonstrates the conjugation-enhancing effect of the alkoxy substituents (replaced here by hydroxy groups for simplicity). The rotational barrier of **2** is about twice the thermal energy at 164 K. This means even at this temperature we have to take into account a distribution of rotationally hot molecules, and in most solid solutions we will observe a distribution of frozen non-equilibrium geometries. The TDDFT calculations predict the converged absorption wavelength at a larger number of repetition units than suggested by the experimental data. Torsional motion diminishes the π-electron overlap and reduces the conjugation length, which explains the increasing difference between the calculated and experimental absorption wavelengths with increasing degrees of rotational motions. Another consequence is the substantial bathochromic absorption shift with decreasing temperature.

The absorption maxima of **M** and **D** at 77 K (Fig. S1, supplementary material) are located in the red edge or extreme red edge of of the polymer absorption at room temperature. Therefrom, we conclude that torsional motion of aromatic units restricts conjugation to less than

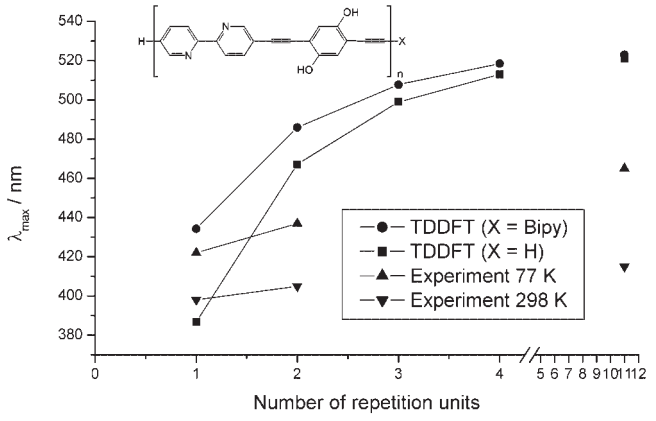

Figure 2. Convergence of the absorption wavelength: comparison between theory and experiment

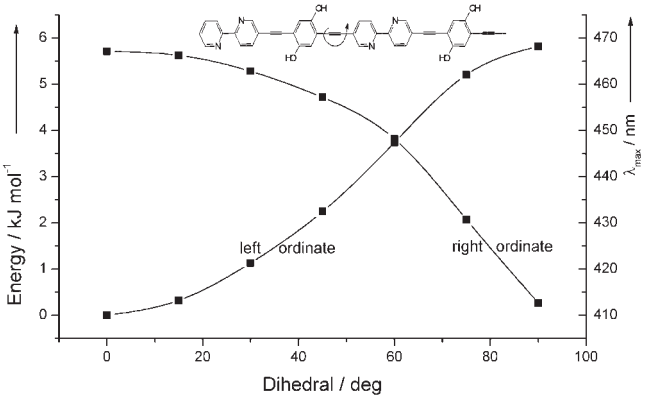

Figure 3. Energy profile for the rotational motion around an ethynylene linkage and its effect on the position of the longest wavelength absorption

Table 2. Rotational relaxation times, stationary and fundamental anisotropies

	M		D		P	
Parameter	Dioxane	$CHCl_3$	Dioxane	$CHCl_3$	Dioxane	$CHCl_3$
ρ_{exp} (ns)[a]	0.65	0.32	2.5	1.3	5–6	9.4
ρ_{calcd} (ns)[b]	0.52	0.24	1.44	0.65	128	
r_0(kin)[a]	0.39	0.35	0.40	0.374	0.33–0.39	
r_{stat}[c]	0.11	0.069	0.25	0.19	0.27	0.24–0.19
r_{kin}[d]	0.127	0.069	0.29	0.22	0.29–0.35	

[a] From TSCP measurements.
[b] $\rho_{calcd} = \eta V/kT$; $V = 4/3\pi a^2 b$.
[c] $r_{stat} = (I_{VV} - I_{VH})/(I_{VV} + 2I_{VH})$.
[d] $r_{kin} = r_0(kin)/(1 + \tau/\rho_{exp})$.

two repetition units in the S_0 state of the polymer at room temperature.

Fluorescence. At room temperature the fluorescence maxima show a moderate Stokes shift, which decreases with increasing chain length (cf. Fig. 1). Again, the band positions and shapes of **D** and **P** differ weakly from each other. The half-widths of the fluorescence bands decrease slightly with increasing chain length, in contrast to those of the absorption spectra. The vibrational structure is better resolved, which confirms the assumption of a more rigid planarized structure of the molecules in the emitting state. On lowering the temperature the absorption and emission spectra become mirror symmetric with a minimal Stokes shift, e.g. 147 cm^{-1} for **D** at 77 K (cf. Fig. S2, supplementary material). The emission maxima undergo only a very small bathochromic shift upon temperature decrease, in marked contrast to the absorption spectra. These findings demonstrate that vibrational relaxation in the excited state produces nearly the same mainly planarized molecular geometry as is occupied on lowering the temperature.

The fluorescence kinetics of all model compounds measured under magic angle conditions is singly exponential and is independent of the emission wavelength. The fluorescence kinetics of the polymers (magic angle) shows small deviations from first-order decay only in the long-wavelength region of the fluorescence band.

The large fluorescence quantum yields and the small lifetimes are due to large radiative and small non-radiative deactivation rate constants (cf. Table 1). With **M** and **D** the radiative rates obtained from $k_f = \Phi_f/\tau_f$ agree well with the k_f calculated from the Strickler–Berg equation. The molar absorptivity of **P** given in Table 1 was determined using the number of repetition units. With this absorptivity, the Strickler–Berg equation predicts a radiative rate constant which is only 40% of the experimental value. If we assume that both k_f agree also for **P**, then we have to assume an effective conjugation length of the emitting chromophore or, in the language of solid-state physics, the size of the exciton, of roughly 2.5 repetition units.

In contrast with the radiative deactivation, the non-radiative deactivation is significantly enhanced from **D** to **P**. Energy migration along the chain is expected to contribute to non-radiative decay in that more quenching sites become available.

Emission anisotropy and energy migration in fluid solution

Energy migration along the polymer chain leads to depolarization of the fluorescence if it goes along with an alteration of the spatial orientation of the transition moment. This cannot occur with the polymer molecules existing as ideal linear rigid rods. We know from frequency and molecular dynamics calculations that we have a distribution of bent conformations in the thermal equilibrium at ambient temperature. Hence investigations into the stationary and time-resolved fluorescence anisotropy in different solvents can deliver information on energy migration. Stationary and fundamental anisotropies r_{stat} and r_0, and rotational relaxation times ρ, are given in Table 2.

The emission anisotropies for **M** and **D** obtained from stationary, r_{stat}, and from time-resolved, r_{kin}, polarization measurements are consistent with each other. The values of r_{stat} and ρ measured in dioxane and chloroform reflect the viscosity ratio. If we calculate the rotational relaxation time from the molecular dimensions according to

$$\rho = \frac{\eta V_{rot}}{kT}, \quad V_{rot} = \frac{4\pi a^2 b}{3}$$

then we obtain a reasonable coincidence with **M** if we neglect the contribution of alkoxy substituents to V_{rot} (V_{rot} = rotational volume; η = viscosity; a and b = long and short half-axis of the molecule, respectively). The reason for using a^2b instead of ab^2 in the above equation is discussed elsewhere.[22] Neglecting the contribution of alkoxy substituents to the rotational volume of **M** means that the rotational diffusion may be interpreted as a revolution around an axle defined by the alkoxy side

groups. With **D**, however, the alkoxy substituents do contribute to the rotational volume, which results in an increased rotational relaxation time. The mechanism of depolarization is a rotation around an axle perpendicular to the long molecular axis for both **M** and **D**. This has to be concluded consistently from the stationary and time-resolved measurements in different solvents and the calculated rotational volumes. The fundamental anisotropy r_0 is 0.39 and 0.40, respectively. That means that the transition moments for absorption and fluorescence are collinear.

For **P** in dioxane, a rotational relaxation time of 128 ns is calculated from the molecular volume, the axial ratio ($a/b = 26.3$) and the solvent viscosity according to the equation given above. Hence the depolarization should be ineffective during the fluorescence liftime of 0.76 ns [$r_{stat} = r_0/(1 + 0.76\,ns/128\,ns) = 0.99\,r_0$]. However, we find experimentally a rotational relaxation time of 5–6 ns and a stationary emission anisotropy of $r_{stat} = 0.27$, which is significantly smaller than $0.99\,r_0 = 0.398$. This means that there must exist another faster depolarization mechanism which is not caused by rotational diffusion of the molecule as a whole. The only reasonable explanation is energy transfer between adjacent chromophores along a bent polymer backbone.

Molecular dynamics calculations, e.g. with an octamer, and emission anisotropies derived therefrom assuming distinct migration distances give evidence that energy migration is restricted to the next-neighbouring chromophore units. Details will be presented in a forthcoming paper.

The anisotropy decay curve for **P** does not extrapolate to $r_0 = 0.4$ whereas those for **M** and **D** do (Fig. S3, supplementary material). This and the limiting anisotropies obtained from Perrin plots give further evidence of a rapid depolarization mechanism not primarily governed by rotational diffusion.

Another proof of the inefficiency of energy migration along the polymer backbone comes from fluorescence quenching experiments with Fe(II), Cu(II) and Ru(II) (Fig. S4, supplementary material). The quenching constants (static quenching) obtained from Stern–Volmer plots for **P** were never found to be larger than twice the value for **M**. This is in marked contrast to the results of Swager and co-workers,[13,14] who demonstrated energy migration over about 50 repetition units of a crown ether-substituted polyphenylenethynylene with the help of fluorescence quenching experiments using paraquat as an electron acceptor.

Absorption, fluorescence and energy transfer in solid films

M, **D** and **P** form transparent glassy films. Whereas films of M crystallize within a few hours after preparation, the polymer films remain glassy for months. In comparison with the solution spectra, the absorption maxima in films are red shifted and display a shoulder or a second less intense absorption peak in the red wing of the long-wavelength band (Fig. S5, supplementary material). These long-wavelength peaks correspond to those of the solution at low temperatures. Temperature reduction not only gradually reduces torsional motion but also favours aggregation, which mutually requires planarizations. Also π–π stacking interaction may give rise to a bathochromic shift. In the crystal **M** shows a card-pack stacking with an unusually large intermolecular distance of 614 pm (H. Görls, personal communication, 2002). If aggregates in solution exhibit a similiar geometry to the molecular stack in the crystal, then one should expect from exciton theory a hypsochromically shifted absorption maximum (H-aggregate) and a vanishing fluorescence quantum yield. The longest wavelength absorption peaks of dissolved **M** at 77 K and of crystalline **M** at room temperature coincide. Although comparatively weak, the fluorescence is also observable in the film. Hence we conclude that the π–π interaction is small in the ground state and the temperature effect on the spectra is mainly due to the freezing of torsional motion. The molecular packing in the solid state has a similar effect to temperature reduction in that it favours more and larger more planarized species or chain segments giving rise to longer wavelength absorption peaks Theory also predicts the weakness of the π–π interaction. DFT calculations with an aggregate of two molecules of **1** (X = bipy) using the geometry from the crystal structure predict an attracting interaction of 0.6 kJ mol^{-1}. RHF calculations with the aug-cc-pVDZ basis set predict a repulsive interaction of 1 kJ mol^{-1}.

The fluorescence properties change more than the absorption features when comparing the solution with the film. Apart from being red shifted, the fluorescence spectra are broadened and less structured. The fluorescence intensity is strongly diminuished by roughly two orders of magnitude. The fluorescence kinetics are no longer singly exponential and they slow with increasing detection wavelength (Fig. S6, supplementary material). The decay is faster in the short-wavelength region and slower in the long-wavelength region of the emission band in comparison with the (wavelength-independent) decay in solutions. We have to conclude from the close similarity of the decay curves for **M** and **P** that the same type of intermolecular interaction is responsible for the slowing with increasing wavelength.

Obviously, in the films of **M**, **D** and **P** more than one different emitting species exist. The species emitting in the short-wavelength region undergo additional deactivation in comparison with the solution, which is again faster for the polymer than for the model compounds. However, in the long-wavelength region the decay is dominated by species with longer lifetimes which are nearly the same for **M** and **P**.

We are led to suppose from distribution analyses of the emission kinetics (cf. Fig. S7, supplementary material)

that the fluorescence behaviour in the glassy film is not determined by distinct species or aggregates. The experimental data indicate that in films different emitting chromophores exist in a more or less broad distribution which undergo very effective radiationless deactivation. This should be due to the enhanced internal conversion in the aggregates itself and/or intermolecular energy transfer in connection with quenching sites. From the mutual orientation of two **M** molecules in the crystal and from the spectral data, we calculate the energy transfer rate along the stacking direction according to the Foerster mechanism as $2.2 \times 10^{14}\,s^{-1}$. Even between adjacent stacks the rate is as high as $1.7 \times 10^{12}\,s^{-1}$. We may safely expect similar transfer rates at least for crystalline domains of the neat polymer.

In order to investigate the role of energy transfer in the quenching process, rhodamine B octadecyl ester (**RhBE**) was used as an additional energy acceptor for sensitization experiments with **P** as the donor. This dye shows good spectral overlap of its absorption with the fluorescence of **P**. Furthermore, the absorption spectra of the donor and the acceptor are well separated to allow selective excitation of either compound (Fig. S8, supplementary material). The absorption spectrum of the mixture is a linear superposition of both components, hence there is essentially no interaction in the ground state. No fluorescence is detectable with the **P** film when exciting in the **RhBE** absorption region, nor is any excitation intensity measurable in the region of the rhodamine absorption when taking the fluorescence from the **RhBE** emission region. Neat films of **RhBE** show fully matching absorption and excitation spectra with no hints of impurities or aggregation. Excitation in the region of the donor absorptions yields a negligibly small emission signal. The fluorescence spectra of the film containing both **P** and **RhBE** (Fig. S9, supplementary material) give strong evidence of an energy transfer from **P** to **RhBE**. Excitation of the polymer results in a decrease in the polymer fluorescence together with a marked increase in the acceptor fluorescence. In particular, the significantly lower directly excited rhodamine fluorescence in comparison with the more intense fluorescence observed upon irradiation into the polymer absorption proves the energy transfer. The same conclusion can be drawn from the excitation spectra. The excitation spectrum of the rhodamine fluorescence is significantly more intense in the region of the polymer absorption than in the region of the **RhBE** absorption.

The mean fluorescence lifetime of **P** is shortened from 0.83 to 0.47 ns. This gives evidence of a non-trivial energy transfer, although the lifetimes are somewhat uncertain because of low count rates. Whether intermediate energy migration along several donor molecules is involved in the energy transfer from **P** to **RhBE** requires further investigation.

In order to study the influence of intermolecular interaction on the spectral properties in more detail, we have

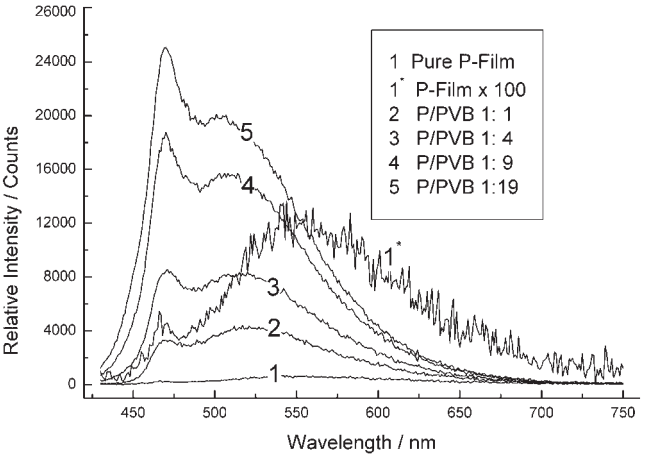

Figure 4. Emission spectra from a series of films of **P** in PVBu in comparison with pure **P**

additionally investigated pure films of **P** and series of solid solutions of **P** in poly(vinyl butyral) (**PVBu**) with varying mass ratio (Fig. 4). The absorption spectra of spin cast films characterized by a maximum at 455 nm and a broad band between 440 and 390 nm do not show any systematic variation with the polymer concentration. This means that aggregation and π–π stacking interaction do not cause spectroscopically significant effects in the ground state. The bathochromic absorption shift with respect to the solution is essentially due to restricted rotation and a more extended coplanar conformation of chain segments. This conclusion is confirmed by the close similiarity of absorption recorded at 77 K in methylcyclohexane–cumene with the room temperature absorption of the film.

In marked contrast to the absorption spectra, the fluorescence spectra of the films depend significantly on the **P** concentration. The overall fluorescence quantum yield of **P** is highest at the lowest concentration (**P** : **PVBu** 1 : 19) and decreases systematically by roughly two orders of magnitude for the pure **P** film. The band shape varies also systematically with increasing **P** concentration in that the broad long wavelength emission increases at the expence of the narrow emission band at 470 nm. The emission spectrum of **P** in **PVBu** solution at highest dilution differs from that in fluid solution by a bathochromic shift of 11 nm of the maximum. The changes of the emission spectra as a function of **P** concentration are comparatively more pronounced. These observations also rule out that the concentration invariance of the absorption spectra might be due to a phase segregation of the polymer mixture.

Obviously, there are two emitting types of species, (i) non-interacting polymer backbone chromophores which essentially determine the character of the solution spectrum and (ii) an excimer-like species which gives rise to the broad long-wavelength emission. The intensity increase of the excimer emission with increasing concentration of **P** becomes particularly evident from the difference spectra (not shown) obtained by subtracting

the emission spectra of the sample with the lowest concentration from all other ones after normalizing all spectra to unity at 470 nm. The emission spectra are independent of the excitation wavelength and the excitation spectra do not depend on the emission wavelength, which means that both emissions originate from the same absorbing species in accord with the excimer hypothesis.

CONCLUSIONS

Poly{2,2′-bipyridine-5,5′-diylethynylene[2,5-di(2-ethylhexyl)oxy-1,4-phenylene]ethynylene} and its 'monomer' and 'dimer' model compounds are highly fluorescent in solution. The excitation energy in the S_1 state of the polymer is delocalized over not more than about 2–3 repetition units. Torsional motion of aromatic chain constituents prevent a larger conjugation length, which is predicted from theory to be roughly twice as large. Temperature reduction produces essentially the same molecular coplanar chain segments in the ground state as vibrational relaxation in the excited state. Intermolecular π–π stacking interaction is negligibly small in the ground state both in solution and in solid films. Planarization of larger chain segments due to temperature reduction or to the molecular packing in the solid state allow the formation of excimer species upon excitation. Energy migration along the polymer backbone is inefficient. Intermolecular excitation energy transfer, however, is efficient. This explains the reduction of the fluorescence quantum yield with the polymer in solid films. In spite of the short excited state lifetime of the polymer, it can efficiently sensitize an embedded rhodamine dye. Hence, among others, this type of polymer deserves further consideration as antenna chromophores for solar energy conversion.

Acknowledgements

We cordially thank Dr H. Görner, Mülheim, for a gift of DCS and Professor R. Sauerbrey for putting the Ti–sapphire laser source at our disposal. We are particularly grateful to Dr H. Görls for making the crystal structure of **M** accessible to us.

REFERENCES

1. (a) Bunz UHF. *Chem Rev.* 2000; **100**: 1605–1644; (b) Bunz UHF. *Acc. Chem. Res*. 2001; **34**: 998–1010; (c) Friend RH. *Pure Appl. Chem*. 2001; **73**: 423–425.
2. Brabec J, Sariciftci NS. In *Semiconducting Polymers*, Hadzioannou G, van Hutten PF (eds). Wiley-VCH: Weinheim, 2000; 515–560.
3. Schumm JS, Pearson DL, Tour JM. *Angew. Chem*. 1994; **106**: 1445–1448.
4. Yamamoto T, Yamada W, Tagaki N, Kizu K, Maruyama T, Ooba N, Tomaru S, Kurihara T, Kaino T, Kubota K. *Macromolecules* 1994; **27**: 6620–6626.
5. Wautelet P, Moroni M, Oswald L, Le Moigne J, Pham A, Bigot J-Y, Luzzati S. *Macromolecules* 1996; **29**: 446–455.
6. Nalwa HS. In *Handbook of Organic Conductive Molecules and Polymers*, vol. 4, Nalwa HS (ed). Wiley: Chichester, 1997; 261–361.
7. Balzani V, Juris A, Venturi M. *Chem Rev.* 1996; **96**: 759–833.
8. (a) Ley KD, Whittle CE, Bartberger MD, Schanze KS. *J. Am. Chem. Soc.* 1997; **119**: 3423–3424; (b) Ley KD, Schanze KS. *Coord. Chem. Rev.* 1998; **171**: 287–307.
9. Grummt U-W, Birckner E, Klemm E, Egbe DAM, Heise B. *J. Phys. Org. Chem.* 2000; **13**: 112–126.
10. Grummt U-W, Birckner E, Al-Higari M, Egbe DAM, Klemm E. *J. Fluoresc*. 2001; **11**: 41–51.
11. Birckner E, Grummt U-W, Göller AH, Pautzsch T, Egbe DAM, Al-Higary M, Klemm E. *J. Phys. Chem.* 2001; **105**: 10307–10315.
12. Liu G. *Macromolecules* 1993; **26**: 5687–5962.
13. Swager TM, Gil CG, Wrighton MS. *J. Phys. Chem.* 1995; **99**: 4886–4893.
14. Zhou Q, Swager TM. *J. Am. Chem. Soc.* 1995; **117**: 12593–12602.
15. Martin RE, Diederich F. *Angew. Chem*. 1999; **111**: 1420–1469.
16. Pautzsch Th, Klemm E. *Macromolecules* 2002; **35**: 1569–1575.
17. Demas JN, Crosby GA. *J. Phys. Chem.* 1971; **75**: 991–1024.
18. Lakowicz JR, Gryczynski I, Laczko G, Gloyna D. *J. Fluoresc*. 1991; **1**: 87–93.
19. Lakowicz JR. *Principles of Fluorescence Spectroscopy* (2nd edn). Kluwer Academic/Plenum Publishers: New York, 1999; 298–299.
20. Frisch MJ, Trucks GW, Schlegel HB, Scuseria GE, Robb MA, Cheeseman JR, Zakrzewski VG, Montgomery JA Jr, Stratmann RE, Burant JC, Dapprich S, Millam JM, Daniels AD, Kudin KN, Strain MC, Farkas O, Tomasi J, Barone V, Cossi M, Cammi R, Mennucci B, Pomelli C, Adamo C, Clifford S, Ochterski J, Petersson GA, Ayala PY, Cui Q, Morokuma K, Malick DK, Rabuck AD, Raghavachari K, Foresman JB, Cioslowski J, Ortiz JV, Baboul AG, Stefanov BB, Liu G, Liashenko A, Piskorz P, Komaromi I, Gomperts R, Martin RK, Fox, DJ, Keith T, Al-Laham MA, Peng CY, Nanayakkara A, Gonzalez C, Challacombe M, Gill PMW, Johnson B, Chen W, Wong MW, Andres JL, Gonzalez C, Head-Gordon M, Replogle ES, Pople JA. *Gaussian 98, Revision A.7*. Gaussian: Pittsburgh, PA, 1998.
21. Göller A, Grummt U-W, Birckner E, Klemm E, Egbe DAM. *Int. J. Quantum Chem*. 2001; **84**: 86–98.
22. Birckner E, Grummt U-W. *J. Fuoresc*. submitted.

